JAMECH
Vol. 46, No. 2, July 2015, pp 221- 231

A Computational study on the effect of different design parameters on the accuracy of biopsy procedure

Zahra Matin Ghahfarokhi[1], Mehdi Salmani Tehrani[1], Mahdi Moghimi Zand[2*] and Mojtaba Mahzoon[3]

1. Department of Mechanical Engineering, Isfahan University of Technology, Isfahan, Iran

2. School of Mechanical Engineering, College of Engineering, University of Tehran, Tehran, Iran

3. Department of Mechanical Engineering, University of Shiraz, Shiraz, Iran

Received: 30 April 2015; Accepted: 22 July 2015

Abstract

Needle insertion is a minimally invasive technique in diagnosing and treating tumors. However, to perform a surgery accurately, the tissue should have minimum amount of displacement during needle insertion so that it reaches the target tissue. Therefore, the tissue membrane has to move less to decrease rupturing under the membrane. In this study, the effect of different design parameters on displacement of the point where a puncture occurs during needle insertion is investigated. Finite element simulation is used to study the effect of mechanical properties of the tissues (hyper-viscoelastic coefficients) and geometric parameters of the needle (fillet radius, needle tip angle and needle diameter) and friction coefficient. To validate the simulations, the results were compared with previously published results in the literature, i.e. the hyper-viscoelastic properties of brain tissue in neurosurgical procedure and the hyper-viscoelastic properties of liver tissue. The results show that the hyper-viscoelastic constitutive is a suitable model to describe soft tissue behavior. Also, the mechanical properties of the tissue and needle velocity are effective on the displacement of the tissue's membrane and therefore in surgery accuracy.

Keywords: *finite element simulation, hyper-viscoelastic model, needle insertion, soft tissue.*

1. Introduction

Many modern clinical practices are done in therapy centers. These practices involve percutaneous diagnosis and local therapies. In this method, a needle, probe or similar objects have to be inserted into soft and inhomogeneous tissues to reach a target with the aid of biopsy and brachytherapy. Since soft tissues exhibit anisotropic and time/rate dependent behavior, needle insertion into a soft issue leads to changes in organ shape and

* Corresponding Author: Tel.: +98-21-61114807; Fax: +98-21-88013029, Email Address: mahdimoghimi@ut.ac.ir

hence in the position of the target. But, the needle tip must be accurately placed on the target tumor. This is a major challenge in such practices. Therefore, many researches have focused on modeling and simulating the organ deformations that may occur during needle insertion [1-7].

Some researchers have dealt with developing an efficient material model to simulate deformation of a special organ. For example, Miller [8] developed a simple linear viscoelastic model for brain tissues. In this model, the strain energy function was used in the form of convolution integral with the coefficient expressed in the exponential series form [8]. The stress and strain rates are strongly dependent on the proposed viscoelastic model. This model can be applied to large scale finite element computations with ABAQUS software. Sharifi Sedeh [9] proposed a hyper-viscoelastic and quasi-linear model for bovine liver. The model was used to accommodate realistic tissue properties such as large deformation within an FE model. To describe the viscoelastic and nonlinear properties of material, Kobayashi [4] developed a material model. He used the experimental results to validate his model. However, Kobayashi's model includes many parameters and is very complex. Due to different behavior of soft tissues under tension/ compression and shear loading, numerous researchers, such as Miller and Rashid [10-12] have investigated these areas.

Miller proposed a number of hyper-viscoelastic models for brain tissue under uniaxial compression in vitro/in vivo at low strain rates. These models were based on the strain energy function in polynomial form with time dependent coefficients [11]. One of the advantages of the proposed models is that the constitutive equation developed here is suitable for large scale computation and available in ABAQUS software [11, 13].

Among other investigations in this field, Rashid et al. [12] conducted experimental tests in various loadings. They used shear test at different strain rates to determine the mechanical properties of porcine brain tissues. Their results show that the Moony-Rivilin is a linear shear response model and coincides with linear experimental shear data as observed at strain rates used in the tests. However, Ogden's model is suitable for both linear and nonlinear experimental shear data. However, the limitation of this study is that material parameters variable in the strain energy functions are based on average mechanical properties of the brain tissue. Keep in mind that many constitutive models are unsatisfactory since most of the models investigate tissue behavior in vitro while tissue response in vivo differs in vitro.

Liver biopsy involves needle insertion into the liver to diagnose cancer and other diseases. A tissue cutting procedure is affected by puncture, friction or cutting through heterogeneous tissues [6, 14, 15]. Numerous studies have attempted to investigate effective characteristics of needle on the cutting/friction force and their distribution under needle insertion. For example, needle insertion experiments into bovine liver are used to establish the relation between the specific cutting force and the cutting edge angle [16]. Han et al. [14] determined the optimal rotation/ translation speed and the desired tip configuration. They demonstrated that when the bevel angle increases at low rotation/ translation ratios, slice/push ratio becomes very small thus making it suitable for rotational needle biopsy. Okamura et al. [3] investigated the effect of needle diameter and tip type on insertion force and found a significant effect of tip type on insertion forces. Sharifi Sedeh [9] optimized the place of needle insertion. Sharifi Sedeh et al. estimated the time of needle insertion into tissue, and then used MATLAB® program to optimally place the angle of needle insertion. During needle-based procedures, transitions between tissue layers often involve puncture events that lead to sudden rupture events involving layer forces and tissue deformations and unstable crack extensions due to tissue inhomogeneity (contrary to what is experienced in homogeneous tissue phantoms) and changes in structures that affect energy flow into the tissue cracks [17-21]. It is commonly known that faster motions of a needle cause less tissue deformation during cutting and penetration of a biological material [17, 21]. As a result, the lower layer of the tissue is less displaced and the needle accurately inserts into the target tissue. Therefore, crack growth and interaction between needle and tissue need to be explained. On this basis, Gokcol et al. obtained

a fracture toughness of 164±6 J/m^2 for bovine liver [22]. They inserted needles into three samples of livers and investigated the relationship between fracture toughness and needle diameter. Yarpuzlu [23] investigated the correlation between mechanical properties such as viscosity, stiffness/ fracture toughness of bovine liver and histological properties using the Spearman's Rank-Order correlation method. The mechanism of the rupture events during needle insertion into soft tissue was analyzed by Mahvash et al. [17, 21]. They used nonlinear viscoelastic Kelvin model, a stress analysis and the J integral method of fracture mechanics. They showed that faster needle insertion can cause less tissue damage/ force of the rupture event and increase the energy release rate.

Therefore, to study the influence of factors affecting the accuracy of biopsy, mechanical behavior of the soft tissue must be investigated and determined. To this end, this research uses the finite element simulation to investigate the mechanical behavior of brain and liver tissues and to compare the tearing strength of these two tissues. A hyper-viscoelastic model was used as the constitutive model to determine displacement of the point where the needle inserts into the tissue. Then the effect of the needle's geometrical parameters and also mechanical properties of the tissue on insertion time and displacement of the tissue are investigated. The details of simulations and results of this study are presented in the following sections.

2. Constitutive modeling of the soft tissue

This research uses a strain energy based constitutive model for liver and brain tissues. For this purpose, a polynomial form with time-dependent coefficients has been adopted, as proposed by Miller [8] and Sharifi Sedeh et al. [9]. Then the coefficients for the model were determined to be applicable for a special soft tissue.

These models are suitable and available to simulate with models which are suitable and available to simulate with the ABAQUS software. Tissue's time-dependent behavior can be modeled by strain energy function (w) for the hyper-viscoelastic material. The strain energy can be written as follows [8]:

$$w = \int_0^t \left\{ \sum_{i+j=1}^{N} \left[C_{ij0} \left(1 - \sum_{k=1}^{N} g_k \left(1 - e^{\frac{-(t-\tau)}{\tau_k}} \right) \right) \right] \times \frac{d}{d\tau} \left[(J_1 - 3)^i (J_2 - 3)^j \right] \right\} d\tau \quad (1)$$

In this equation, τ is the time variable, τ_k is the characteristic time, t characterizes the duration (time), g_k governs the relaxation coefficient (k=1, 2), the coefficients C_{ij0} describes hyperelastic constants, J_1, J_2 and J_3 are invariants of left Cauchy–Green deformation tensor , given by Equation (2) and N indicates the order of the polynomial in terms of J_i invariants.

$$\begin{aligned} J_1 &= \text{trace}(B) \\ J_2 &= \frac{J_1 - \text{trace}(B^2)}{2J_3} \\ J_3 &= \sqrt{\det(B)} \end{aligned} \quad (2)$$

where B is the left Cauchy-Green deformation tensor. If the material is assumed to be incompressible, then:

$$J_3 = 1 \quad (3)$$

The left Cauchy-Green deformation tensor, B, is given by:

$$\mathbf{B} = \begin{bmatrix} \lambda_z^2 & 0 & 0 \\ 0 & \lambda_z^{-1} & 0 \\ 0 & 0 & \lambda_z^{-1} \end{bmatrix} \quad (4)$$

In Equation (4) λ_z denotes for the stretch in the normal direction. Since $J_1 = \lambda_z^2 + 2\lambda_z^{-1}$ and $J_2 = \lambda_z^{-2} + 2\lambda_z$, the only nonzero Piola-Kirchhoff stress component is given by [60]:

$$T_z = \frac{\partial w}{\partial \lambda_z} = \int_0^t \left\{ \sum_{i+j=1}^{N} \left[C_{ij0} \left(1 - \sum_{k=1}^{N} g_k \left(1 - e^{\frac{-(t-\tau)}{\tau_k}} \right) \right) \right] \times \frac{d}{d\tau} \left(\frac{\partial}{\partial \lambda_z} (J_1 - 3)^i (J_2 - 3)^j \right) \right\} d\tau \quad (5)$$

Appling this equation and assuming N=2, a very good agreement between the theory and experiments results can be achieved. Therefore:

$$T_z \int_0^t \left\{ \left(1 - \sum_{k=1}^{N} g_k \left(1 - e^{\frac{-(t-\tau)}{\tau k}} \right) \right) \times \left[C_{200} \frac{d}{d\tau} \left(2\lambda_z - 2\lambda_z^{-2} \right) + C_{010} \frac{d}{d\tau} \left(2\lambda_z^{-3} \right) + C_{110} \frac{d}{d\tau} \left(-3 + \lambda_z^2 + 2\lambda_z^{-1} \right) \left(2\lambda_z + \lambda_z^{-2} - 3 \right) \right. \right. \\ \left. \left. + C_{200} \frac{d}{d\tau} \left(-3 + \lambda_z^2 + 2\lambda_z^{-1} \right) \left(2\lambda_z - 2\lambda_z^{-2} \right) + C_{020} \frac{d}{d\tau} \left(-2\lambda_z^{-2} \right) \left(2\lambda_z + \lambda_z^{-2} - 3 \right) \right] \right\} d\tau \quad (6)$$

Once the constants g, τ and C_{ii0} are obtained from the experimental results, the only nonzero Piola-Kirchhoff component, T_z, can be determined based on Equation (6).

3. Simulation of the uniaxial compression test on the soft tissue

In this section, the experimental tests of uniaxial compression, conducted by Miller [8] and Sharifi Sedeh [24], is simulated to validate ABAQUS simulation results.

Miller [8] used eight samples of swine's brain in his tests. The cylindrical samples in Miller's tests were 30 mm in diameter and 13 mm in height. To determine the model constants, Miller repeated the tests for three different strain rates; 0.64(1/s), 0.64e-2(1/s) and 0.64e-5(1/s). The constants of Miller's model are listed in Table 1.

Table 1. Coefficient hyper-viscoelastic of brain [13]

C_{100}=C_{010} (Pa)	C_{200}=C_{020} (Pa)	g_1	g_2	t_1 (s)	t_2 (s)
263	491	0.45	0.365	0.5	50

Sharfi Sedeh et al. [24] carried out similar tests on bovine liver. They used nine samples of 30-36 mm diameter and 14-19 mm height. Then, to determine the material hyper-viscoelastic coefficients, they repeated the tests at three different strain rates; 0.0011(1/s), 0.0088(1/s) and 0.4167(1/s). Table 2 shows the hyper-viscoelastic coefficients of the liver tissue, obtained in [24]. Since a frictionless contact has been assumed between the rigid plate and cylindrical soft tissue, a homogeneous deformation and therefore a homogeneous stress distribution occurs in the tissue. This means that the stress is equal to force exerted by the plate divided by the cross-section area of the sample. Of course, according to [24], the initial cross-section is used in this research for stress calculation which results in a Piola-Kirchhoff measure of stress. Correspondingly, the strain is calculated as the displacement of the rigid plate divided by initial height of sample.

Table 2. Coefficient hyper-viscoelastic of liver [24]

C_{100}=199.713(Pa), C_{010}=354.897(Pa)
C_{200}=10524(Pa), C_{020}=14792(Pa), C_{110}=436.186(Pa)
g_1=0.5, g_2=0.2917
t_1=0.24(s), t_2=11.3636(s)

The uniaxial compression tests of references [13] and [24] are simulated via a "visco" step, using ABAQUS/Implicit solver. The tissue was meshed using CAX4RH, a four-noded axisymmetric continuum element. Since the tissue is assumed to be incompressible, the hybrid element formulation was chosen. To validate the FE simulations, the stress-strain curves, obtained from present numerical simulations were compared with corresponding experimental results of Miller's tests [8] and [24] in Figures 1 and 2, respectively. As can be seen, a very close relationship between experimental and numerical results is observed. This evidently shows the validity of simulation results.

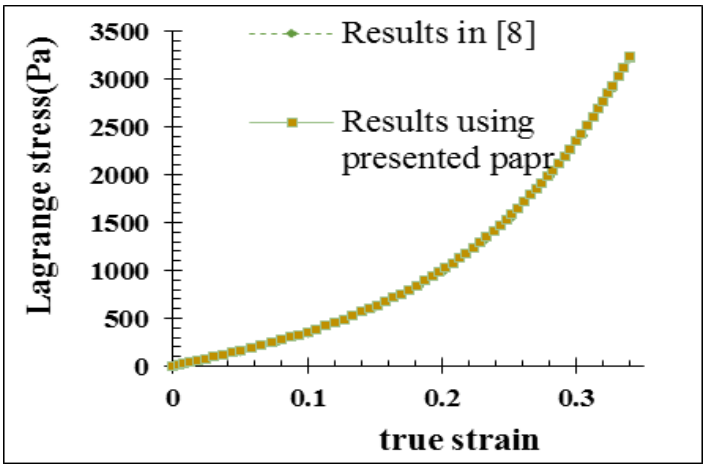

(a)

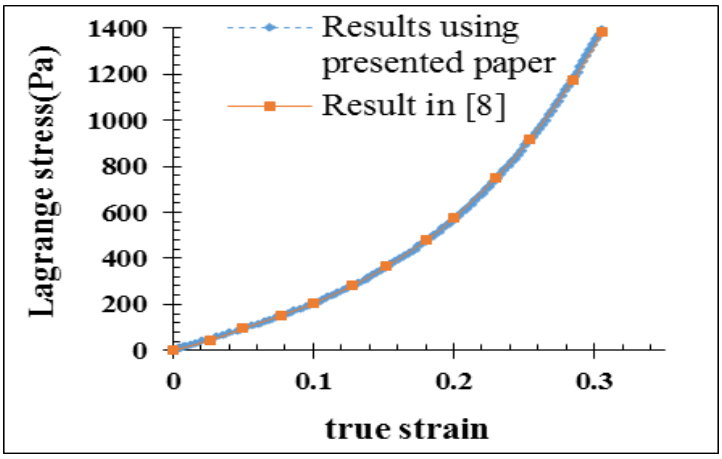

(b)

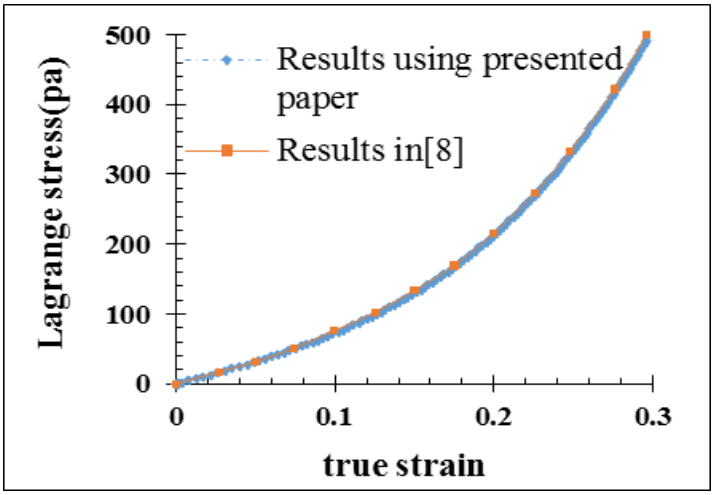

(c)

Fig. 1. Lagrange stress-true strain curves for swine brain (a) loading speed 0.64s^{-1}, (b) loading speed 0.64e-2s^{-1}, (c) loading speed 0.64e-5s^{-1}

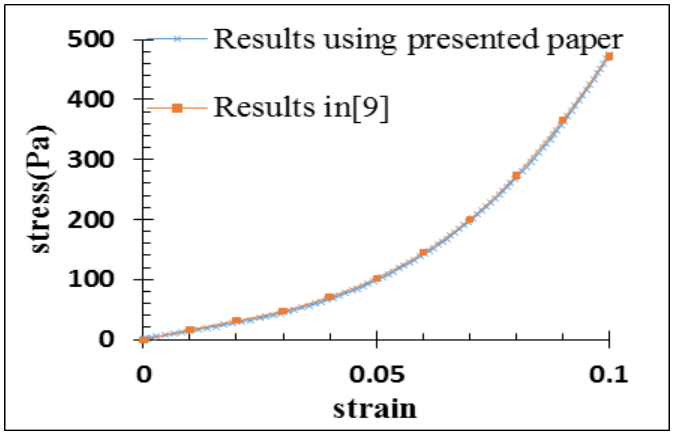

(a)

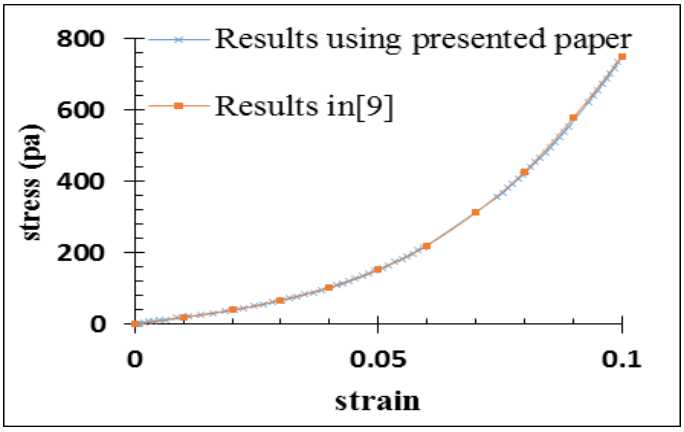

(b)

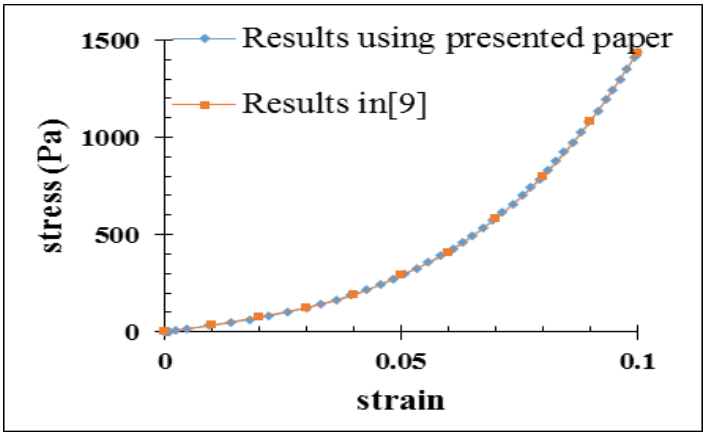

(c)

Fig. 2. Stress-strain relations for bovine liver(a) loading speed 0.0011s^{-1}, (b) loading speed 0.0088s^{-1}, (c) loading speed 0.4167s^{-1}

Now, the effect of needle geometry and mechanical parameters of the tissue on the time which the needle inserts into the tissue and displacement of the point where the needle inserts into the tissue are investigated. To achieve this goal, an axisymmetric modeling was employed using both brain and bovine liver material coefficients. Dimensions of both

models are similar and are as follows: diameter=30(mm), height=13(mm). The compressing load was applied on the model under three different strain rates; 0.64(1/s), 0.64e-2(1/s), and 0.64e-5(1/s). Figure 3 illustrates the Piola-Kirchhoff stress versus true strain for the two materials here considered.

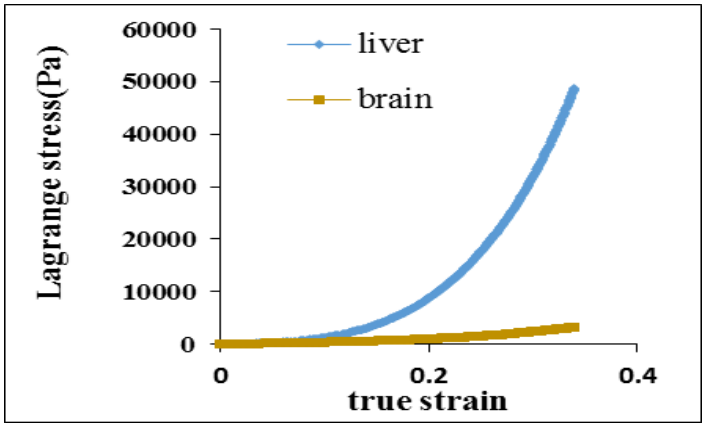

(a)

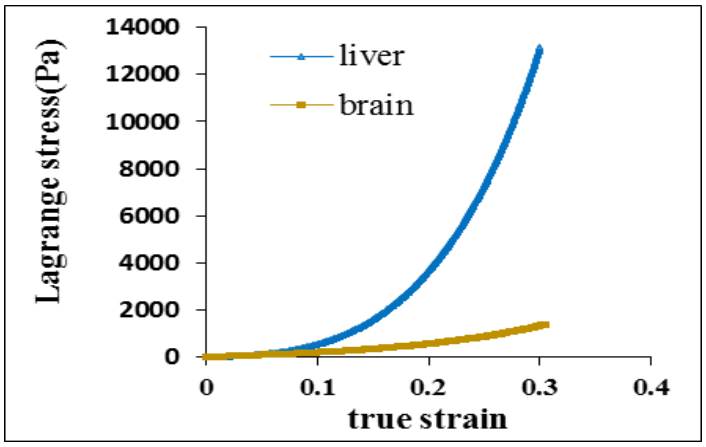

(b)

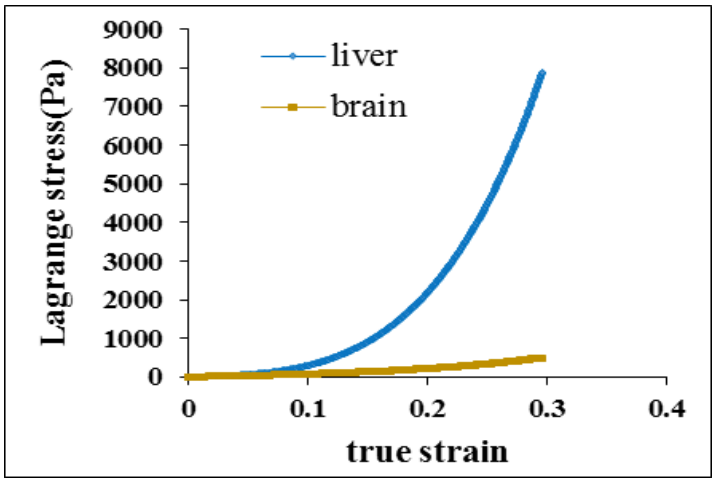

(c)

Fig. 3. Lagrange stress-strain response of brain tissue and liver tissue (a) loading speed 0.64s^{-1}, (b) loading speed 0.64e-2s^{-1}, (c) loading speed 0.64e-5s^{-1}

Now, to simulate needle insertion into the tissue, the brain and liver tissues were modeled as shown in Figure 4. The length and diameter of the needle in Figure 4 are 15.24 mm and 1.27 mm, respectively.

To compare the accuracy of biopsy for the two different tissues, the displacement of the target point, the point where needle is inserted into the tissue, is investigated. For this purpose, the force-displacement curve of the target point for time duration of needle insertion is plotted. These curves are shown in Figure 5. Then, to investigate mechanical and geometric parameters of the needle, needle motion velocity is 0.003 m/s and its fillet radius is 1e-4 m and the friction coefficient between needle and tissue is changed from 0.1 to 0.5. Also, needle diameter changes from 1 to 2.1 mm. Finally, the friction coefficient is kept constant (μ=0.5) and changes in the needle tip angle/ needle fillet radius/ velocity of the needle are investigated. In above steps, the force-displacement responses are shown in Figures 6 to 10. Simulations were stoppedwhen stiffness force reaches 2.3040 N,. a value which is equal with the force required for the needle to puncture the capsule of the liver [9].

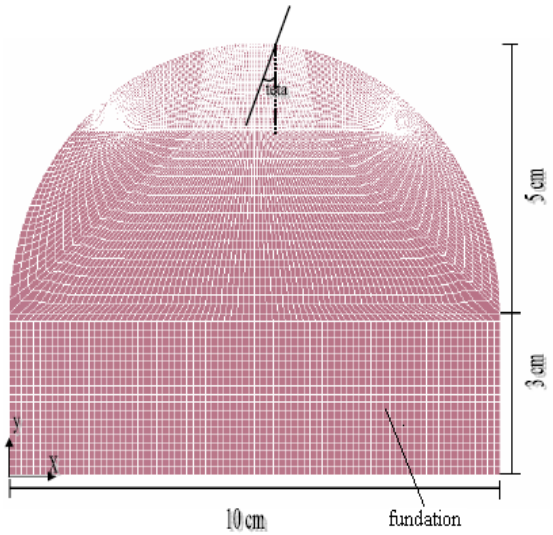

Fig. 4. Dimensions of simulated tissue

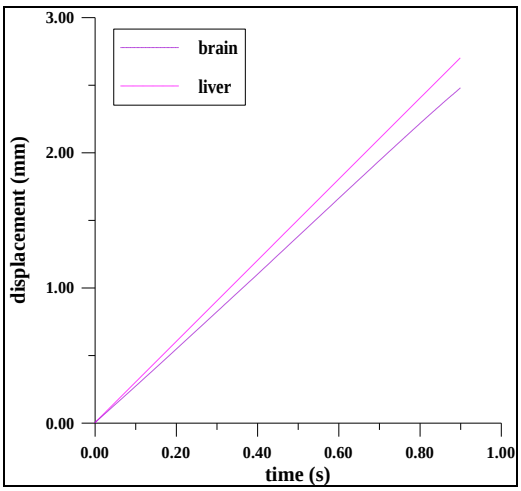

Fig. 5. The stress-strain curves of brain and liver while the needle puncture the tissue

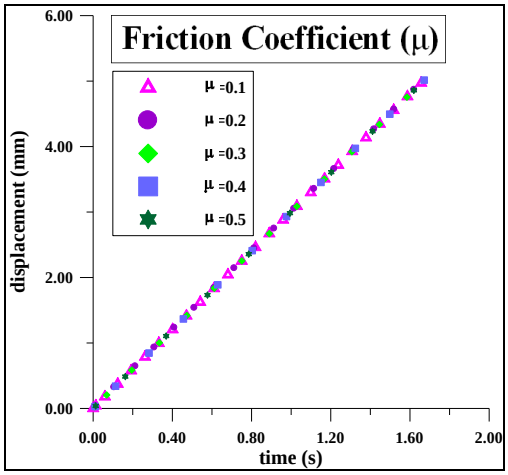

Fig. 6. The variation of displacement of the needle insertion point with changes friction coefficient between needle and tissue

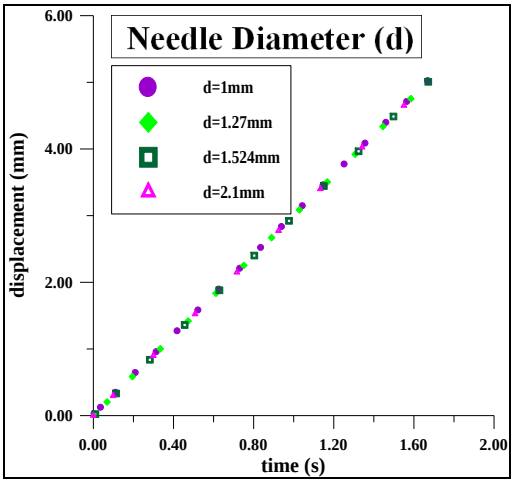

Fig. 7. The variation of displacement of the needle insertion point with changes diameter of needle

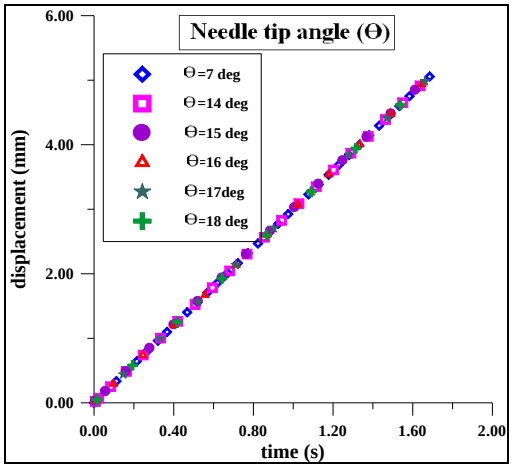

Fig. 8. The variation of displacement of the needle insertion point with changes needle tip angle

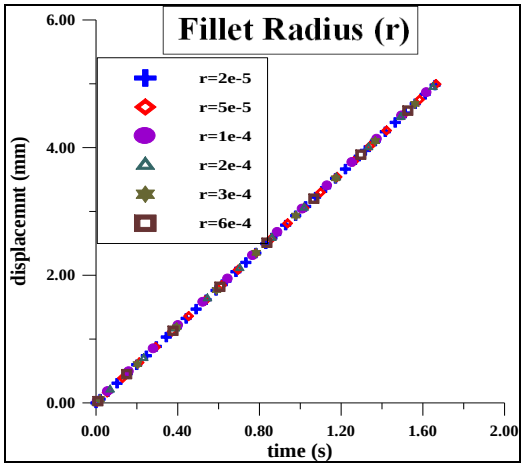

Fig. 9. The variation of displacement of the needle insertion point with changes the needle fillet radius

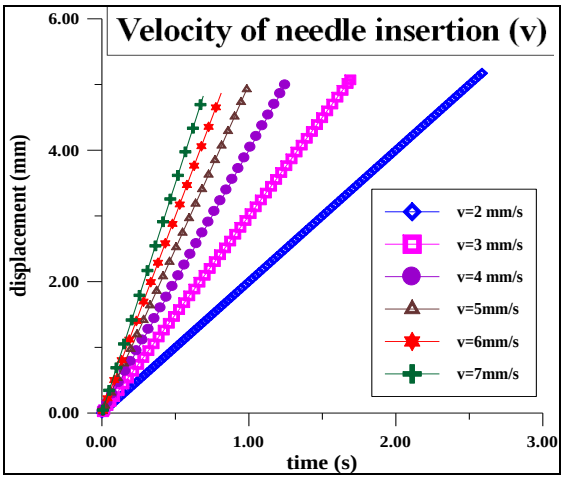

Fig.10. The variation of displacement of the needle insertion point with changes the velocity of needle

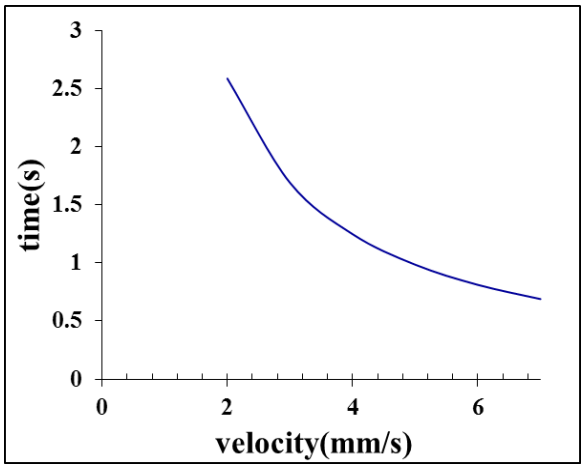

Fig. 11. The variation of time of the needle insertion with changes the velocity of needle

4. Results and Discussion

In this paper, some experimental tests, reported in previously published researches, were simulated to investigate validity of numerical simulations. Comparison between numerical and experimental results for stress-strain curves in Figures 1 and 2 show that numerical simulations are accurate enough to properly predict the deformation of the soft tissue. Piola-Kirchhoff stress against strain curves for different strain rates have been shown in Figure 3. This figure indicates that prior to a strain of 0.1, the stiffness of both liver and brain are the same, for the three strain rates. However, for higher strain values, a significant difference between the two curves can be observed for different strain rates.

In addition, the effects of tissue material parameters on its deformation were investigated. Models were created with liver and brain properties. The variation of displacement-time curve of the point where needle is inserted is shown in Figure 5. Figure 5 indicates that the tissue which has less stiffness, shows more displacement (as expected). Next, parameters affecting the soft tissue and needle on the displacement of the needle insertion point are investigated.

Displacement-time curves associated with different values of needle parameters are shown in Figures 6 to 11. It can be seen that the effects of friction coefficient between needle and tissue, needle diameter, tip angle of the needle and fillet radius of the needle tip on

the displacement-time curve are negligible. However, increasing the velocity of needle movement from 2 to 7 mm/s) leads to decreasing insertion time of the needle into the tissue (Fig. 11) and also 6.77% decreasing displacement of the point where the needle is inserted. The obtained results agree with those reported in the literature.

5. Conclusions

In this article the effects of different design parameters on time and tissue rupture are investigated. For this purpose, finite element simulation was employed to investigate the effects of mechanical properties of the tissue and geometric parameters of the needle. FE simulation results show that the liver tissue has a higher stiffness than the brain's and consequently, the needle needs more time for insertion into the tissue and displacement of its insertion point is less. Since the target point moves less, surgery on this tissue would be more careful. Also, the results show the mechanical properties of the tissue and needle velocity are effective on the displacement of tissue's membrane and accuracy of the surgery. However, other parameters do not have a significant effect on the accuracy of biopsy procedure. Of course it should be noted that high speed also changes the cutting force and friction force. Therefore higher needle speed may not always be better and this must be carefully investigated.

The main novelty of the present work, compared with previously published researches, such as [8] and [24], are thus:

1. In other references, such as [24], a predefined displacement was applied to a special node, rather than needle modeling in the finite element simulation. In other word, the needle was not included in the finite element model, in reference [24]. Therefore the FE model of reference [24] was not able to predict the effect of needle geometry on the deformation characteristics. While in this paper, the needle has been included in the model, as a separate part, and so, the effect of needle geometry has been studied.
2. In addition to investigating needle geometry, the friction coefficient between needle and the tissue and also the material coefficients of the tissue are the other parameters whose effects were studied in the present work were also investigated as they were not considered in previous researches.

References

1. Goksel O., Salcudean S.E., P.Dimaio S., Rohling R., Morris J., 2005, 3D needle-tissue interaction simulation for prostate brachytherapy, Medical Image Computing and Computer-Assisted Intervention, MICCAI.
2. Abolhassani N., Patel R., Moallem M., 2007, Needle insertion into soft tissue: A survey, Med Eng Phys 29: 413-431.
3. Simone C., Okamura A.M., 2002, Modeling of needle insertion forces for robot-assisted percutaneous therapy, in: Proceedings of the IEEE International Conference on Robotics and Automation, Washington, DC, 2085-2091.
4. Kobayashi Y., Watanabe H., Hossi T., Kawamura K., G.Fujie M., 2012, viscoelastic and nonlinear liver modeling for needle insertion simulation, Stus mechanobiol tissue eng biomater 11:41-67.
5. Heverly M., Dupont P., Triedman J., 2005, Trajectory optimization for dynamic needle insertion, in: Proceedings of the IEEE International Conference on Robotics and Automation, 1646-1651.
6. Duriez C., Guebrt C., Marchal M., Cotin S., Grisoni L., 2009, Interactive simulation of flexible needle insertion based on constraint models, Medical Image Computing and Computer-Assisted Intervention, MICCAI.
7. Samur E., Sedef M., Basdogan C., Avtan L., Duzgun O., 2007, A robotic indenter for minimally invasive measurement and characterization of soft tissue response, Medical Image Analysis 11:361-373.
8. Miller K., 1999, Constitutive model of brain tissue suitable for finite element analysis of surgical procedures, J Biomech 32: 531-537.
9. Sharifi Sedeh R., Ahmadian M.T., Janabi Sharifi F. (2010). Modeling, simulation, and optimal initiation planning for needle insertion into the liver, J Biomech Eng 132: 1-11.
10. Miller K., Chinzei K. (2002). Mechanical properties of brain tissue in tension, J Biomech 35: 483-490.
11. Miller K., Chinzei K., Orssengo G., Bendnarz P. (2000). Mechanical properties of brain tissue in-vivo: experiment and computer simulation, J of Biomechanics 33: 1369-1376.
12. Rashid B., Destrade M., D.Gilchrist M. (2013). Mechanical characterization of brain tissue in simple shear at dynamic strain rates, J mech behav biomed mate 28: 71-85.
13. Miller K., Chinzei K. (1997). Constitutive modeling of brain tissue: experiment and theory, J Biomech 30(11/12): 1115-1121.

14. Han P., Ehmann K. (2013). Study of the effect of cannula rotation on tissue cutting for needle biopsy, Med Eng Phys 35: 1584-1590.
15. M.Okamura A., Simone C., D. O'Leary M. (2004). Force modeling for needle insertion into soft tissue, In: Proceedings of the IEEE transactions biomedical engineering 51(10): 1707-1716.
16. Z.Moore J., Malukhin K., J.Shin A., F.Ehmann K. (2011). Hollow needle tissue insertion force model, CIRP Ann Manuf Technol 60: 157-160.
17. Mahvash M., E.Dupont P. (2009). Fast needle insertionto minimize tissue deformation and damage, in: Proceedings of the IEEE International conference on robotics and automation, Kobe, Japan, 3097-3102.
18. Atkins A.G., Mai Y.W. (1985). Elastic and plastic fracture: metals, polymers, ceramics, composites, biological materials, Chichester: Ellis Halsted Press, 1st ed.
19. Lathrop A., Smith R., Webster R. (2008). Needle-membrane puncture mechanics, in: Proceedings of the International conference medical image computer assisted intervention , MICCAI.
20. Mahvash M., Hayward V. (2001). Haptic rendering of cutting, a fracture mechanics approach. Haptics-e, Electron J Haptics Res 2(3): 1-12.
21. Mahvash M., E.Dupont P. (2010). Mechanics of Dynamic needle insertion into a biological material, IEEE Transactions biomedical engineering 57(4): 934-943.
22. Gokgol C., Basdogan C., Canadinc D. (2012). Estimation of fracture toughness of liver tissue: experiments and validation, Med Eng Phys 34: 882-891.
23. Yarpuzlu B., Ayyildiz M., Enis Tok O., Ranan Gulhan A., Cagatay B. (2014). Correltion between the mechanical and histological properties of liver tissue, J Mech Behav Biomed Mater 29: 403-416.
24. Sharifi Sedeh R. (2005). Online control of needle injection in haptic devices into soft tissue using finite element method, MS thesis, Sharif University of technology, Iran (in Persian).